PNL-SA-6698

CONF-780430--7

# Krypton Entrapment in Pulse Biased Sputter-Deposited Metals

Pacific Northwest Laboratory
Richland, Washington 99352
Operated for the
U.S. Department of Energy by

Battelle
Memorial Institute

PNL-SA-6698

## DISCLAIMER

# KRYPTON ENTRAPMENT IN PULSE BIASED SPUTTER-DEPOSITED METALS

by

M. A. Bayne, R. W. Moss,

and E. D. McClanahan

Battelle Northwest Laboratories

Richland, Washington 99352



Prepared for the U.S. Department of Energy
Under Contract EY-76-C-06-1830

Contributed for presented at the Third International Conference on Metallurgical Coatings, sponsored by the American Vacuum Society, in San Francisco, CA, on April 3 through April 7, 1978.

# KRYPTON ENTRAPMENT IN PULSE BIASED SPUTTER-DEPOSITED METALS*

M.A. Bayne, R.W. Moss, and E.D. McClanahan

Battelle Northwest Laboratories, Richland, Washington 99352

A supported gas discharge sputtering system was constructed to investigate krypton entrapment in high-rate sputter-deposited thick films. Krypton entrapment was studied as a function of substrate and target voltage for nickel, aluminum, titanium and iron deposits. Control of substrate and target voltages was achieved with pulse circuits capable of adjusting the pulse duration and repetition rate. A water-cooled cylindrical copper substrate 15 cm in diameter was used to collect the sputtered metal from a 9-cm diameter cylindrical target. To observe the immediate effect of changes in sputtering parameters on gas trapping, as well as measure the total gas trapped, a sensitive mass flow indicator was installed in the krypton supply of the dynamically pumped system. Data relating krypton content to substrate bias conditions and deposition rate are discussed in light of the theory of Carter, Colligon and Leck on ion absorption in the presence of sputtering. Krypton contents > 2 at.% were found in the metals studied, all of which were deposited at rates exceeding 1 nm/sec. Computed krypton concentrations agreed with concentrations in samples that were analyzed chemically.

---

## 1. INTRODUCTION

Radioactive $^{85}Kr$ is a fission product with a relatively small impact upon man.[1] However, because a reduction in all radioactive emissions from nuclear facilities is desirable, storage of this off-gas may be required.[2] Laser[3] summarizes the work being done world-wide on the separation, storage and disposal of $^{85}Kr$. To provide an alternative to pressurized cylinder storage, the entrapment of the gas in a metal matrix by sputter-deposition is being investigated. Although gas incorporation by this means is not new,[4,5] high rate sputter deposition was selected for further development in the United States because of its low pressure, low temperature characteristics when compared with other $^{85}Kr$ storage alternatives such as

*Prepared for the U.S. Department of Energy Under Contract EY-76-C-06-1830.

encapsulation in an aluminosilicate matrix, which requires high temperatures and pressures.[6] Other characteristics of high-rate sputtering, as developed at Battelle's Pacific Northwest Laboratories, which are particularly adaptable to this application are: 1) a high strength substrate bond, 2) reproducible deposits through the control of the sputtering parameters and the use of computerized instrumentation, 3) deposition of unconventional materials with desirable properties, 4) independently variable power densities on the target and substrate electrodes, and 5) long-term reliability and stability. However, the greatest impact is that large surface area, thick coatings, may be deposited at rates considerably higher than those normally associated with sputtering while maintaining the large substrate ion current densities necessary for high trapping rates. High volume, commercial application then becomes feasible.

This paper reviews the basic theory of ionic trapping in a receding surface and how it is presently applied. Specific data for ion entrapment in mild steel, aluminum, nickel and titanium prepared by high-rate, supported discharge sputter deposition are presented.

## 2. THEORETICAL

Carter, Colligon and Leck[3] utilized a probability of sorbtion function, $\rho$, to derive equations for the sticking probability of an ion in a solid:

$$\omega_s = \int_0^{\lambda} \rho(\xi)d\xi \leq 1, \qquad (1)$$

the number of gas atoms sorbed up to a time, t, in a receding surface:

$$N_{Ti} = \frac{B}{v}\left[\psi(o)-\psi(vt)+\sigma(\lambda)vt\right] \quad [\text{atoms/cm}^2], \qquad (2)$$

and the maximum number of ions that may be sorbed in a receding surface:

$$N_{Ts} = \frac{B}{v}\left[\psi(o)-\psi(\lambda) + \sigma(\lambda)\lambda\right] \quad [\text{atoms/cm}^2], \qquad (3)$$

where $\lambda$ = maximum ion penetration depth [cm]
$\xi$ = x-vt
= relation between the distance from the instaneous surface at a time, t, and the distance from the initial surface
B = ion current flux density [ions/cm$^2$/sec]
v = surface recession rate [cm/sec]
$\sigma(x) = \int p(x)dx$
$\psi(x) = \int \sigma(x)dx$

In the pulsed-bias mode of trapping, when the substrate bias is applied, the substrate is experiencing a net removal of material, even though metal atoms may be arriving from the target if it is being operated continuously and atoms are also being redeposited from the substrate on the portion of the substrate not masked by the target. Then for equations (2) and (3), if the target is operating continuously,

$$v = \frac{B}{n}\left[S(E_S)(1-f_2) - f_1\, S(E_T)A_T/A_S\right] \qquad \text{[cm/sec]} \qquad (4a)$$

or if the target is "shut-off" while the substrate is "turned-on",

$$v = \frac{B}{n} S(E_S)\,(1-f_2) \qquad \text{[cm/sec]} \qquad (4b)$$

where $n$ = solid atomic volume [atoms/cm$^3$]
$S$ = sputtering yield
$f_1$ = system material transfer efficiency factor
$f_2$ = fraction of material removed from substrate that is redeposited on the substrate
$E_S$ = substrate bias voltage
$E_T$ = target bias voltage
$A_S$ = substrate area
$A_T$ = target area

Also, since for each cycle one must replace the material removed during the substrate "on" pulse and provide a fresh layer of material for the next cycle, approximately

$$N_{MSUB} = 2Bt_S S(E_S)A_S(1-f_2) \qquad \text{[atoms]} \qquad (5)$$

must be deposited.

Therefore,

$$N_{MSUB} = N_{MTAR} = f_1 Bt_T S(E_T)A_T \qquad \text{[atoms]} \qquad (6)$$

Also, if the target is operating continuously, the period of one cycle is

$$P = t_T \qquad (7a)$$

or, if intermittently,

$$P = t_S + t_T \qquad (7b)$$

If the ion dose, $Bt_S \ll B\lambda/v$, then

$$\omega_S \sim \left.\frac{dN_{Ti}}{d(Bt)}\right|_{t_S \ll \frac{\lambda}{\bar{v}}} \qquad \text{[atoms/ion]} \qquad (8)$$

so that the gas incorporation rate is

$$R_1 \sim \frac{\omega_S A_S B t_S}{P} \qquad \text{[atoms/sec]} \quad (9)$$

If the deposit is previously loaded with gas, the substrate bias is applied continuously, and the target is not biased, the gas release rate from the substrate is

$$R_2 = -f_3 n v A_S \qquad \text{[atoms/sec]} \quad (10)$$

where $f_3$ is the fraction of gas in the deposit.

This is assuming bombardment induced re-emission is the major process since operation is in the large bombardment rate and high gas content regime.

## 3. EXPERIMENTAL PROCEDURE

### 3.1 General

The sputtering apparatus designed for this project was of the triode or supported discharge type. The general arrangement is shown in Figure 1. The cylindrical substrate, fabricated from 6-inch copper pipe, was utilized as part of the vacuum chamber wall to facilitate water cooling. For short experiments, the substrate was lined with 0.11 mm thick nickel sheet to aid in sample removal for analysis. The hardware shown was mounted on a standard BNW base assembly containing the electron source, power and cooling water connections, and the pumpout port. The centrally located, water cooled target was fabricated from nickel, steel, aluminum or titanium rod or double extra strong mild steel pipe and was attached via an electrically insulated fitting through the base assembly. The gas inlet valve is a Veeco PV-10, controlled automatically to maintain a constant pressure near the electron source. The flowmeter is a Hastings-Raydist Model ALL-5 with a 0-6.95 ± 0.14 $cm^3$/min rating at STP for krypton. Typical sputtering parameters are given in Table 1. The dependent variables are krypton gas flow rate and material deposition rate at the substrate. The ratio of these two variables is the instantaneous concentration of krypton in the metal. To obtain the flow rate, the baseline due to the throughput of the dynamically pumped system is substracted from the flow-meter indication. After multiplying by the meter sensitivity factor for Kr (1.39), the gas incorporation rate of the deposit is obtained directly in $cm^3$/min at STP. The deposition rate is obtained by calculating the material arrival rate at the substrate utilizing the sputtering yield, geometrical transfer factors and sputtering parameters of the system. The calculation provides the average deposition rate in grams/min,

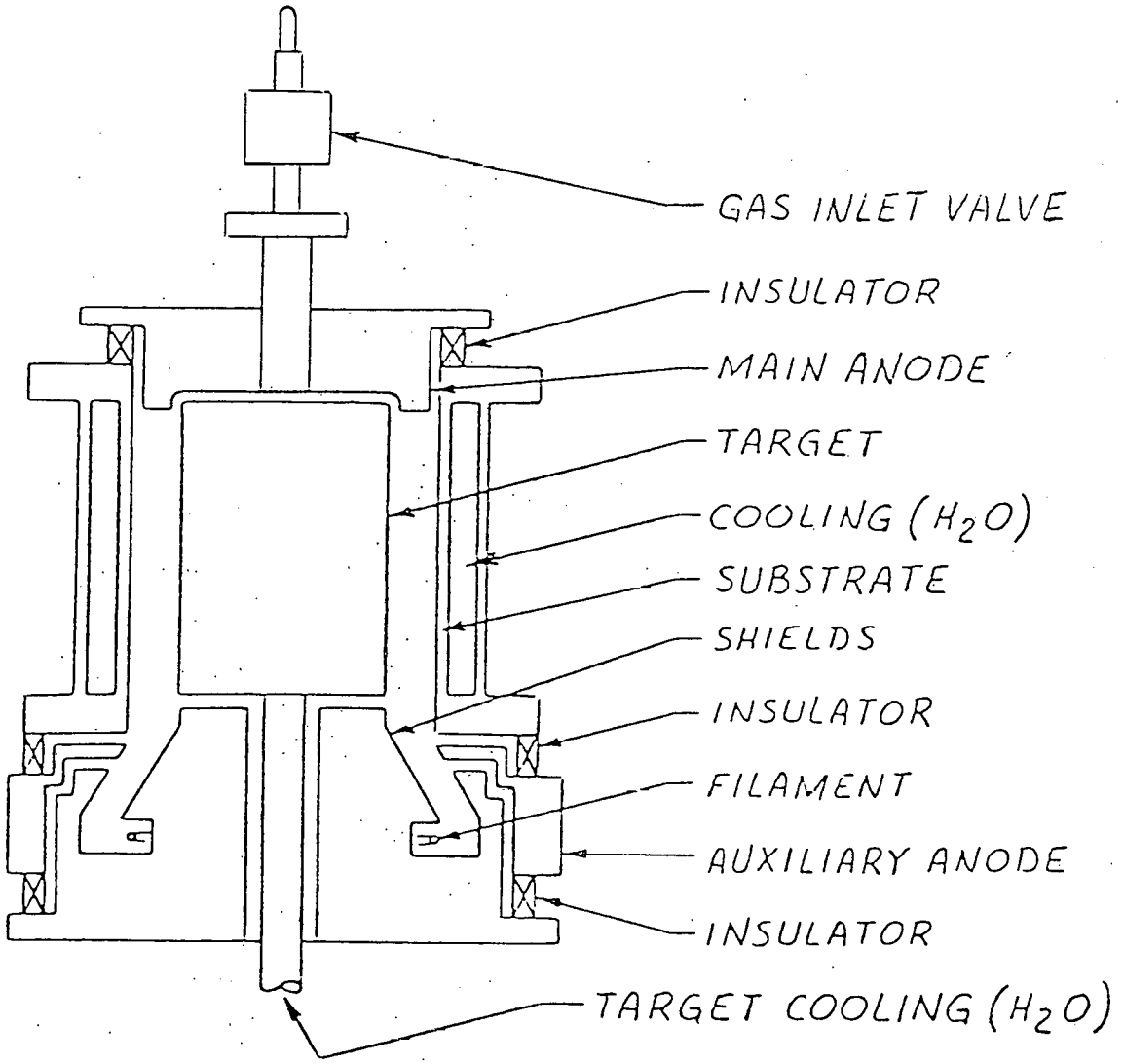


Fig. 1. Coaxial cylinders sputtering geometry for krypton entrapment by high rate sputtering. The target diameter is 10 cm. The substrate diameter is 15 cm.

so that the concentration is obtained. The actual gas content at a particular position on the substrate is determined after an experiment by gas fusion analysis or x-ray flouresence spectroscopy since end effects dominate most of the existing substrate area. The average gas content for an entire experiment is calculated by integrating the krypton flow and dividing by the substrate weight gain.

TABLE I. Typical Deposition Parameters

Auxiliary Anode to Filament Voltage: -30v
Auxiliary Anode to Main Anode Voltage: +7v
Auxiliary Anode to Target Voltage: -2.5Kv
Auxiliary Anode to Substrate Voltage: -2.5Kv
Filament to Main Anode Electron Current: 50 amps
Filament to Auxiliary Anode Electron Current: 5 amps
Target Ion Current: 4 amps
Substrate Ion Current: 7 amps
Auxiliary Anode to Ground: 0 ohms
Shields to Ground: 150 ohms
Krypton Pressure: 0.40 Pa ($3 \times 10^{-3}$ Torr)
Substrate pulse, $t_S$: 6 msec.
Period: 24 msec.

## 3.2 Substrate Bias

Because of the geometry of our system (concentric cylinders), the maximum bias voltage one may continuously apply to the substrate must stay below a definite level to insure a net deposition. For the materials studied, this value is much less than the value required to have a krypton-ion ($Kr^+$) sticking coefficient, $\omega_S$, greater than 0.1 atoms/ion. Therefore, it was necessary to develop procedures to allow the substrate bias voltage to be easily and quickly switched. Two procedures were used. The first involved modification of the substrate arc-limiting circuitry to allow external control. This produced square waveforms with independently variable period and pulse duration, fig. 2a.

The second involved utilization of the three-phase feature of the substrate bias power supply to produce half-wave rectified waveforms as shown in fig 2b, c, d. The latter was investigated primarily as simplifications for future production applications.

2a. Square-wave

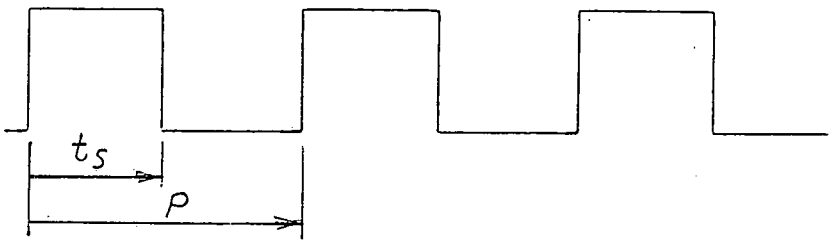


2b. Half-wave rectified, one phase

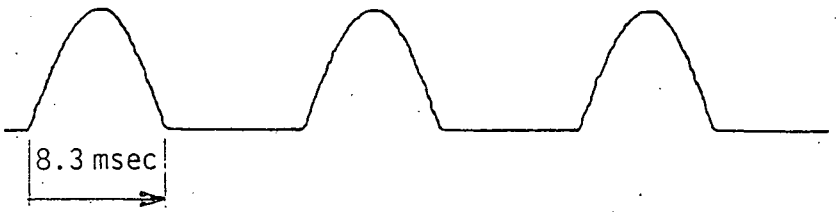


2c. Half-wave rectified, two phases


2d. Half-wave rectified, three phases


Fig. 2. Substrate-bias waveforms that were investigated.

After a substrate etch at 100 volts for 100mA-sec/cm$^2$, the target voltage is raised to full value at the rate of 40 volts/min. Then the substrate bias is slowly increased until the maximum flow rate is attained. By adjusting $t_S$, P and $E_S$, R is maximized. During the diagnostic and sputtering parameter optimization phases of this work, information about the sticking coefficient of these metals was also obtained.

## 4. RESULTS AND DISCUSSION

### 4.1 Sputtering Yields

To evaluate the results and optimize the use of electric power for gas trapping, accurate sputtering yield values are necessary. Krypton sputtering yields for iron and nickel are available in the range of 100-600 eV. To extend the range of the yield measurements to 2500 eV $Kr^+$ ions, the apparatus shown in figure 3 was fitted with 3.8 cm diameter targets of nickel and A-108 steel, the same alloys used in the gas trapping work. The deposition parameters are listed in Table II along with the yields $S/(1+\gamma)$ by ion energy. The yield data are computed from weight measurements and ion dose received for each ion energy. The results are excellent extrapolations of Rosenberg & Wehner's data[9].

TABLE II: Krypton Sputtering Yield Experimental Parameters and Data

| Material | Target Voltage (volts) | Yield $s/(1+\gamma)$ (atoms/ion) | Target Current (mamps) | Plasma Current (amps) | Plasma Voltage (volts) | Pressure (pascals) |
|---|---|---|---|---|---|---|
| Nickel | 1500 | 2.73 | 100 | 15.0 | 42 | 0.25 |
| " | 2000 | 3.53 | 100 | 12.0 | 40 | 0.24 |
| " | 2500 | 3.94 | 100 | 9.1 | 40 | 0.29 |
| Steel | 500 | 1.03 | 100 | 11.2 | 40 | 0.23 |
| " | 1000 | 1.77 | 100 | 10.9 | 40 | 0.25 |
| " | 1500 | 2.29 | 100 | 10.8 | 40 | 0.28 |
| " | 2000 | 2.69 | 100 | 10.1 | 40 | 0.28 |
| " | 2500 | 2.85 | 100 | 11.7 | 40 | 0.28 |

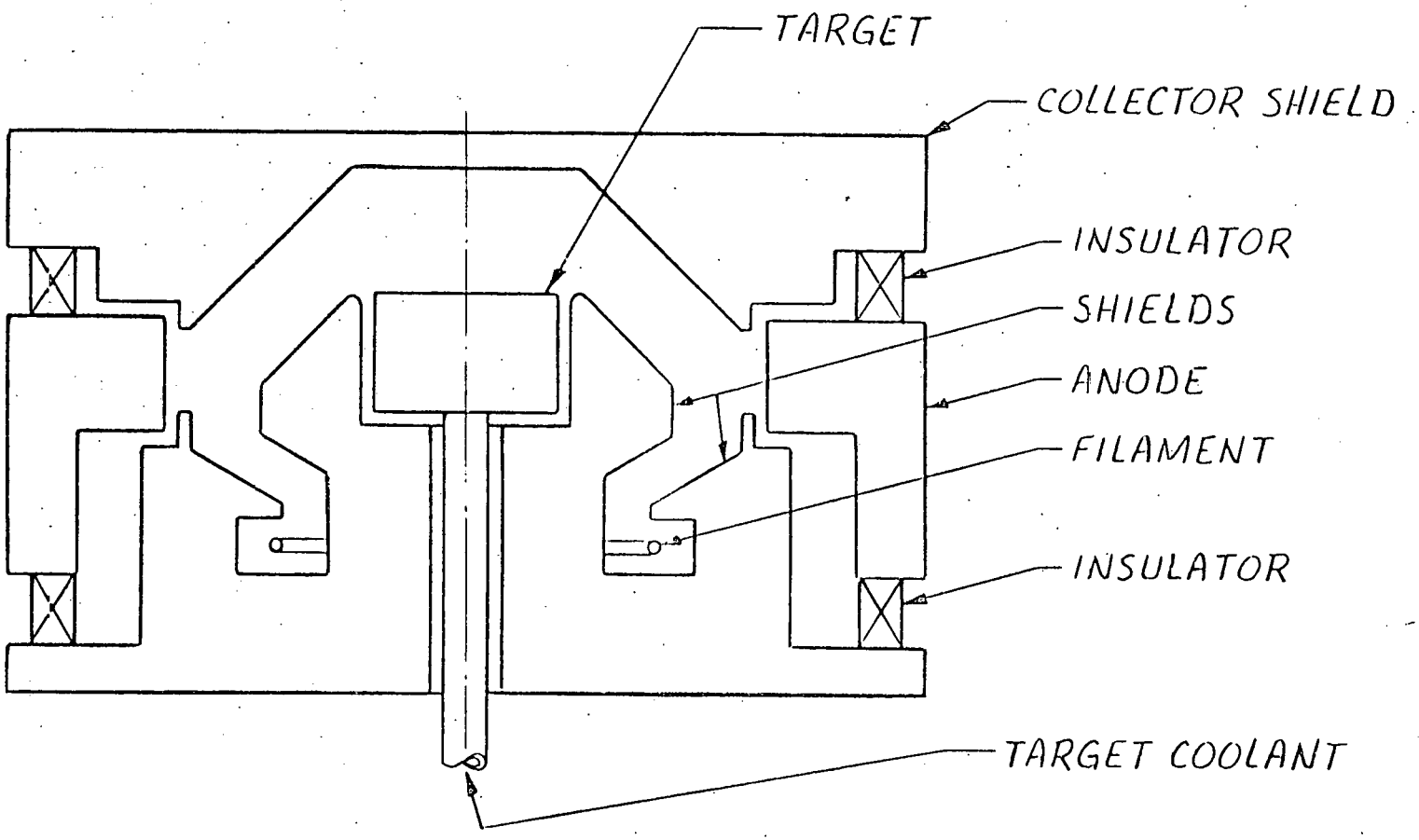


Fig. 3. Sputtering yield measurement apparatus. All electrodes and shields are water cooled. The target diameter is 4 cm.

## 4.2 Gas Entrapment

By manipulating the deposition parameters, deposits with relatively high gas loadings were prepared. The overall results are presented in Table III. Although the nickel deposit for this single experiment was 271 grams, a series of experiments were made consecutively on the same substrate until a total mass of 744 grams was obtained containing 10.4 liters (STP) of krypton. A close-out layer of 210 grams of nickel not containing gas was then deposited to aid in gas retention at elevated temperatures. Maximum thickness near the center of the substrate was 3.5 mm. Thickness near the top end was 2.2 mm. The thickness profile is presented in figure 4. This profile is also representative for the aluminum, steel and titanium deposits made in the same apparatus.

The highest gas content was obtained in the steel deposit, followed by nickel, aluminum and titanium, Table III. These contents are not maximized and are influenced by both the form of the substrate bias waveform being tested and the end effects of the apparatus. Since the ion sticking probability function, $\omega_S$, is extremely ion-energy dependent in the 0-2500 eV range, the highest average $\omega_S$ values are obtained when the bias is switched on and off as rapidly as possible, producing a square-waveform. The half-wave rectified waveforms produce a fair fraction of ions that strike the substrate with $\omega_S$ values considerably less than maximum, thereby reducing the average striking coefficient. Additionally, they are still sputtering previously deposited material. The half-wave rectified waveforms do tend to provide stable plasma conditions which is an important consideration for production applications.

The initial diagnostics were performed with the square substrate bias waveform to simplify interpretation and to provide increased versatility. By varying the experimental parameters individually, the relationships among the variables in equations 9 and 10 were investigated.

Information about the saturation dose is obtained from figures 5-7 where the number of ions/cm$^2$/cycle incident is plotted against the number of atoms/cm$^2$/cycle being trapped. It is apparent that for both iron and nickel $N_{T_S} > 10^{15}$ atoms/cm$^2$ ($E_S$=2.0KeV) in this mode but that for maximum trapping rate the ion dose per cycle should remain $<10^{16}$ions/cm$^2$. This may be insured by decreasing $t_S$ as the current density is increased. Therefore, high current density is not a limiting factor insofar as ion trapping is concerned.

| Material | Substrate Bias Current Type | Target Bias Current Type | Gas Flow $\frac{cm^3}{min}$ | Deposition Rate nm/sec | Gas Content $\frac{cm^3}{gm}$ | at% | Deposit Mass gm | Min. Release Temp °C |
|---|---|---|---|---|---|---|---|---|
| Nickel | 1500v 7amp Fig.2d | 2500v 4amp continuous | 4.0 | 6.05 | 16.9 | 4.5 | 271 | 600 |
| Aluminum | 1300v 7amp Fig.2b,c | 2700v 4amp continuous | 2.3 | 5.0 | 30.1 | 3.9 | 19.5 | 300 |
| Iron | 2500v 2.2amp Fig.2a | 2500v 1.25amp continuous | 1.74 | 2.65 | 19.8 | 5.1 | 63.7 | 570 |
| Titanium | 2300v 5amp Fig.2b | 2500v 4amp continuous | 1.6 | 4.1 | 17 | 3.7 | 4.2 | --- |

TABLE III. Overall krypton entrapment results.

Fig. 4. Deposit thickness distributions and gas concentration compared with the target/substrate geometrical relationship:

(a) Thickness distribution for a nickel deposit made with less than optimal sputtering parameters. Non-uniform plasma density symptom is small ratio of deposit thickness, top to center. The bottom is thicker than the top because of additional resputtering from the substrate shield and a larger ion current density.

(b) Krypton gas concentration for fig 4(a). Highest gas concentration at the top shows the importance of optimizing the $Bt_S/N_{MTAR}$ ratio. Maximum trapping is not being achieved in the center because of an excessive metal deposition rate. The content remains low near the bottom because for this deposition, $Bt_S$ exceeded $N_{TS}$. Near the top, $Bt_S < 3 \times 10^{16}$ ions/cm$^2$ while near the bottom, $Bt_S > 4 \times 10^{16}$ ions/cm$^2$. The slight rise near the center shows the beginning of the non-uniformity in the current density near the bottom.

(c) Thickness profile for the thick nickel deposit. A uniform plasma density is indicated by the smaller top/center thickness ratio.

Opposite 12

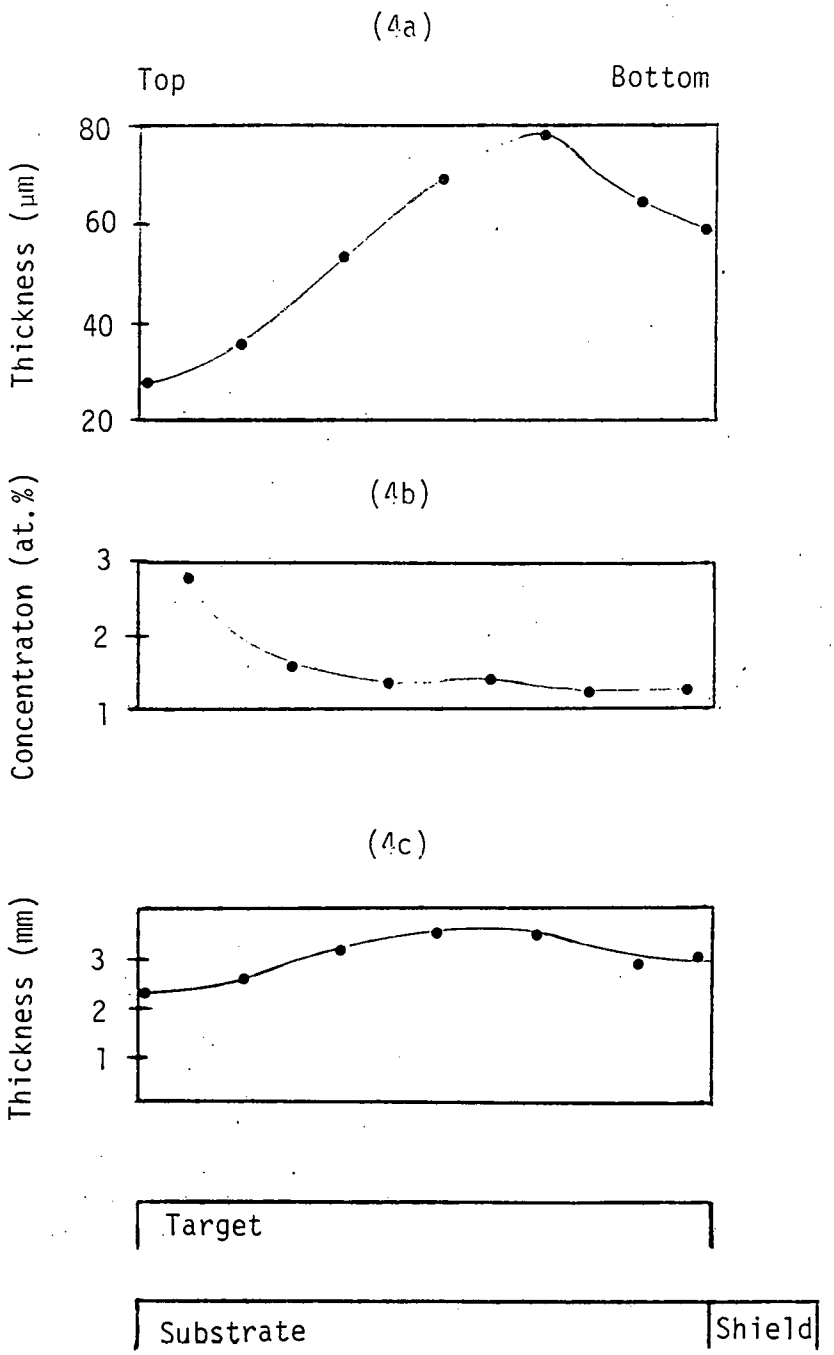
(4a)
Top
Bottom
80
60
40
20
Thickness (μm)
(4b)
3
2
1
Concentraton (at.%)
(4c)
3
2
1
Thickness (mm)
Target
Substrate
Shield

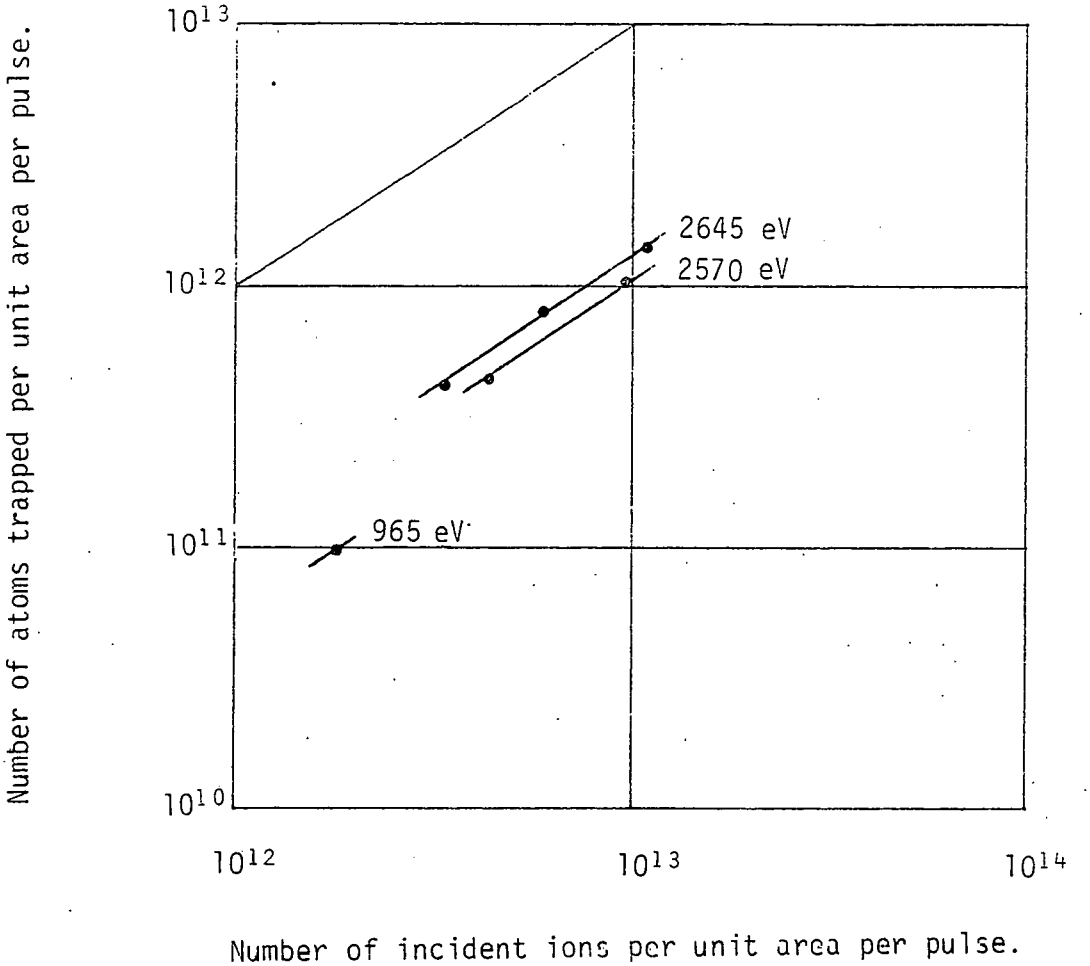


Fig. 5. Variation in the number of krypton atoms trapped as a function of the incident ion dose per cycle with square wave pulses. Material is A-108 steel. The solid line corresponds to $\omega_S = 1$.

---

It is interesting to consider the case where $t_S << \lambda/v$ and P is defined as in equation 7. Then, ions are penetrating much further into the deposit than the thickness of the newly deposited layer. The "internal" dose will approach and could exceed the saturation level described in equation 3 since release of previously trapped gas is inhibited by both the cold water substrate temperature and by the fresh layers of deposited material.

For example, when aluminum is bombarded with 2 KeV $Kr^+$ ions, the maximum penetration depth is $\sim 2 \times 10^{-6}$ cm[10] and by interpolation, the maximum number of atoms trapped, $N_{TS}$, is $\chi$ $2.8 \times 10^{15}$ atoms/cm$^2$ [11], which is a saturation bulk concentration of $1.4 \times 10^{21}$ atoms/cm$^3$, or 2.3 at.%. This gas is distributed similarly to figure 8a. To obtain bulk concentrations higher than 2.3 at.%, one must overlap successive layers of gas as in figures 8b, c. This has been accomplished to some extent

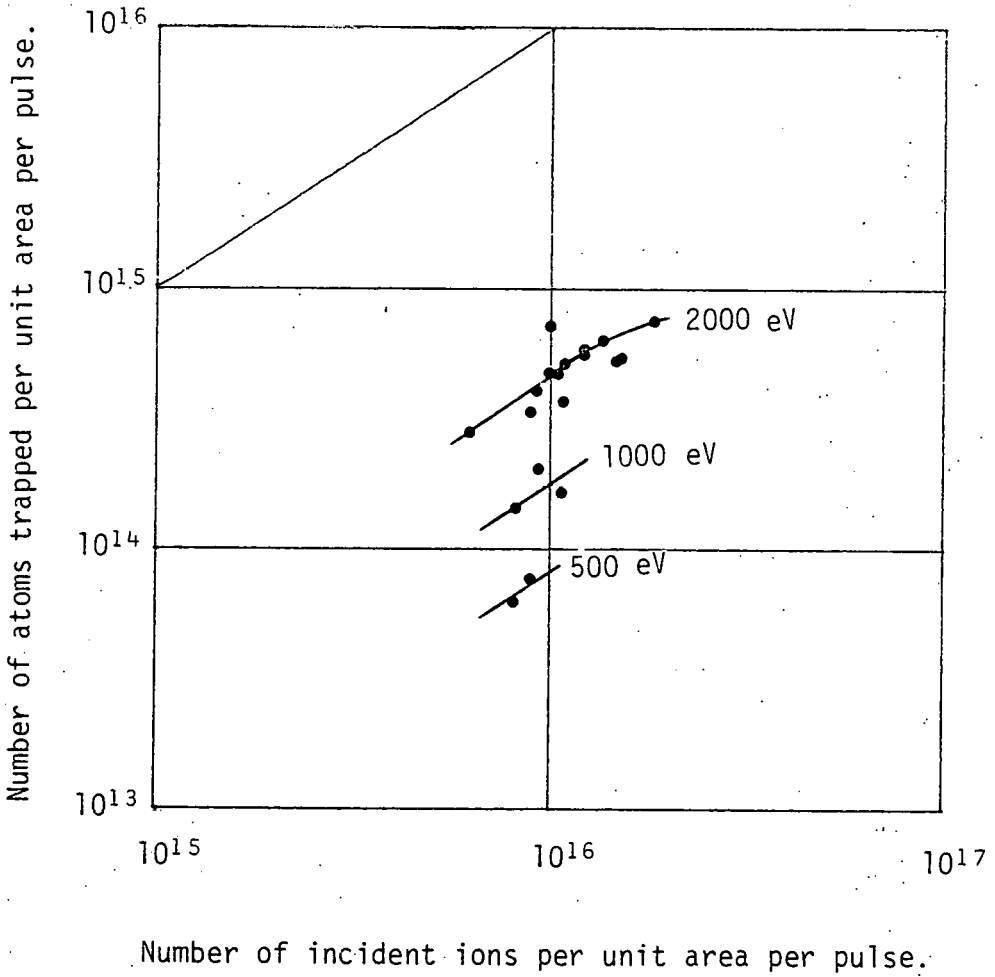


Fig. 6. Variation in the number of krypton atoms trapped as a function of the incident ion dose per cycle with aquare wave pulses. Material is A-108 steel. The solid line corresponds to $\omega_S$=1.

with all the metals tested.

By inspection, one could obtain a deposit with the successive layers overlapped very closely and approach, or exceed the 11.5 at.% indicated as maximum in fig 8a. However, in the present apparatus, end effects are dominant and it is possible to have a positive gas usage rate (equ. 8 ) near the center of the substrate while having a gas usage rate $\leq 0$ near the ends (equ. 9). There would be a transition area adjacent to the ends with a high gas content and the center of

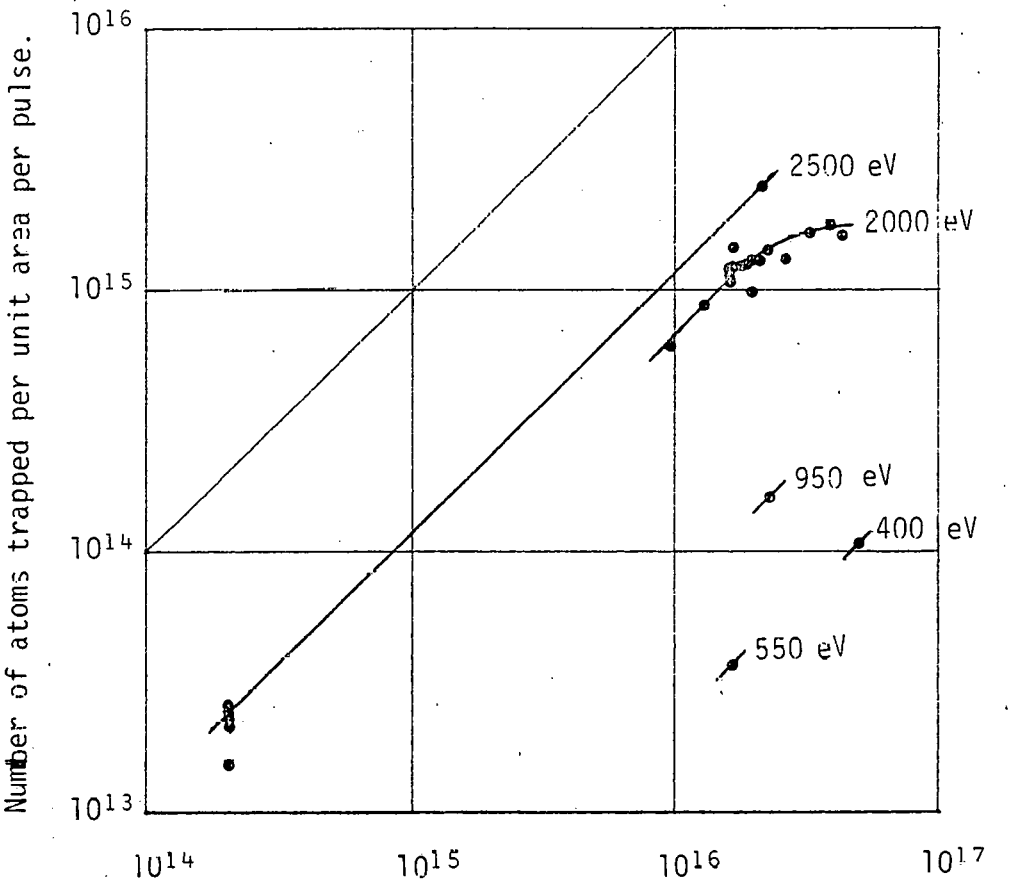


Fig. 7. Variation in the number of krypton atoms trapped as a function of the incident ion dose per cycle with square wave pulses. Material is commercial grade nickel. The solid line corresponds to $\omega_s=1$.

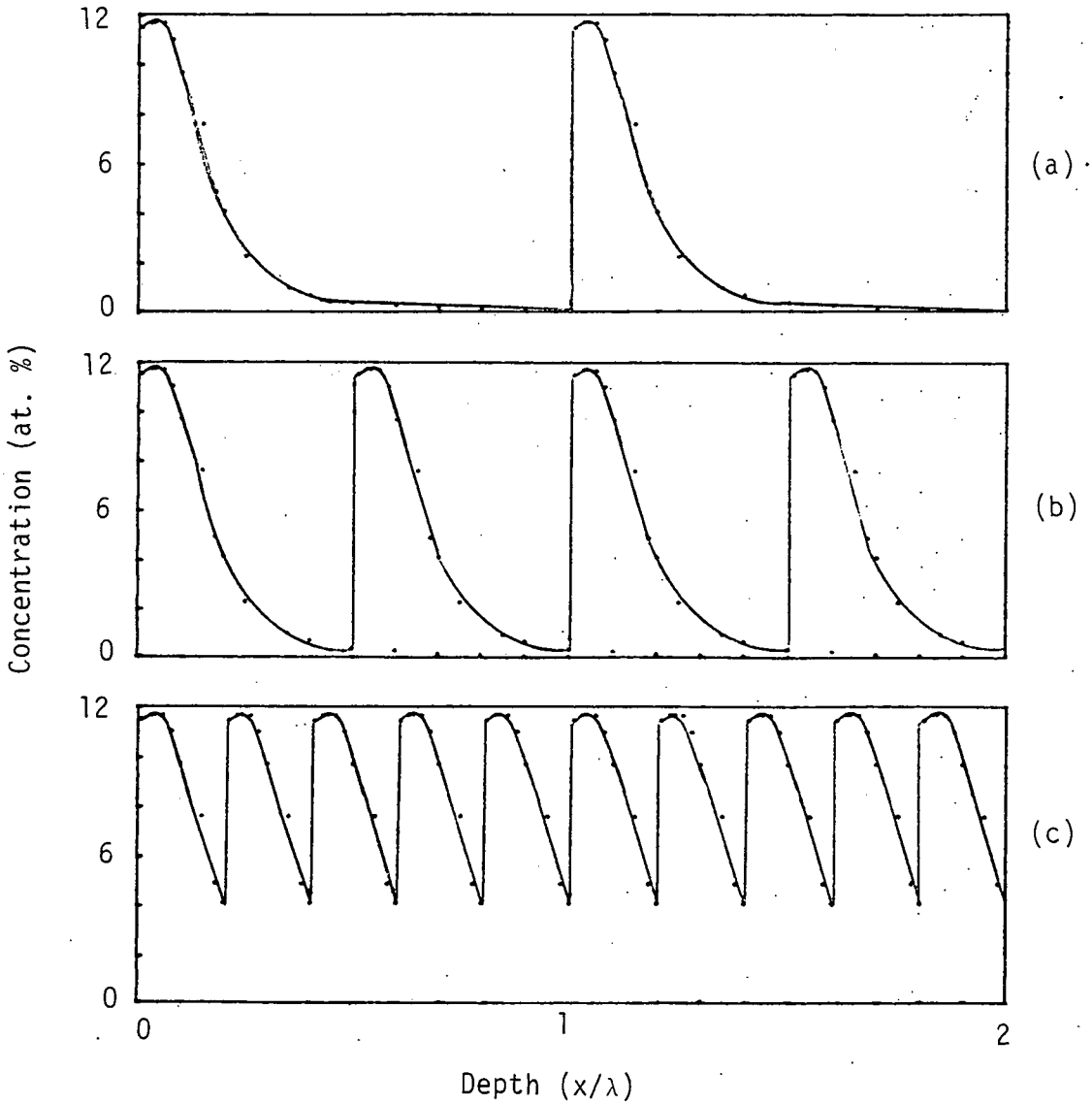


Fig. 8. Atomic concentration of krypton in aluminum as a function of depth for 2 KeV ions. $\lambda$ is maximum penetration depth. Calculated from refs. 8 and 9. $Bt_S=N_{TS}$. (a) Layered deposit with successive gas distributions not overlapped, bulk krypton concentration is 2.3 at.%; (b) layered deposit with successive gas distributions overlapped 50%, bulk krypton concentration is 4.2%; (c) layered deposit with successive gas distributions overlapped 80%, bulk krypton concentration is 9.7%.

the deposit would have a lower gas content because an excessive amount of metal is being deposited to insure that the entire substrate area is trapping gas. This was observed with X-ray flourescent spectroscopy, fig. 9.

The existence of negative gas usage has been observed in two cases:

1) Substrate etch upon resumption of an interrupted deposition

2) Constant $t_S$, B, $E_S$, $E_T$, with decreasing P.

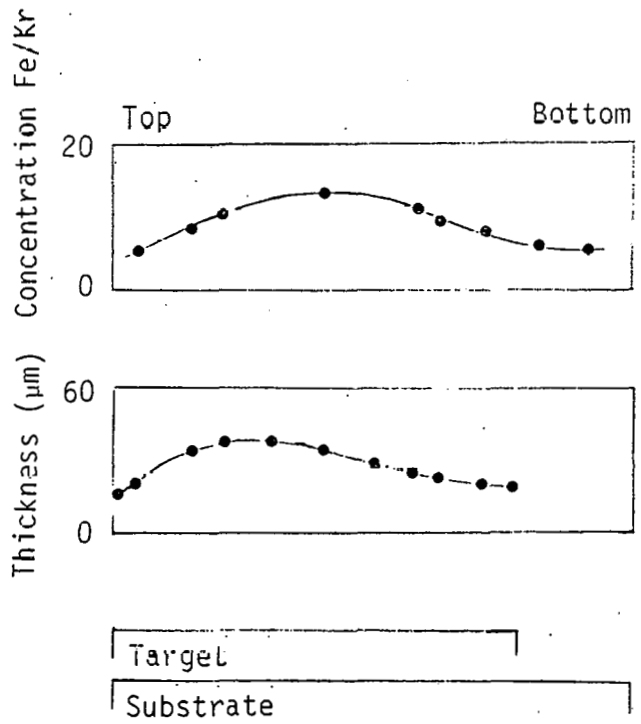


Fig.9. Thickness profile and krypton concentration profile for a steel deposit in relation to the target/substrate geometry. A fairly uniform ion current density is apparent since the maximum thickness is nearly centered on the target. Concentration is Fe/Kr peak height ratio from x-ray florescence data. Notice the reduced krypton concentration near the center and enhanced concentration near the ends.

During the substrate etch, the parameters were

$E_S$ = 100eV
$I_S$ = 3.5 amps
R = -.24 sccm
$f_2$ = .43
Material: Nickel

From equn 9, $f_3$ is 4.4 at.%. For the previous deposition which lasted over 16 hours, the average gas content was also 4.4 at.% calculated from gas usage and deposit weight. Gas usage as a function of period for nickel is plotted in fig 10. Here, $t_S$=6 msec. B=5.5 mA/cm$^2$, $E_S$=$E_T$=2.5KeV and the target is operated intermittently. By

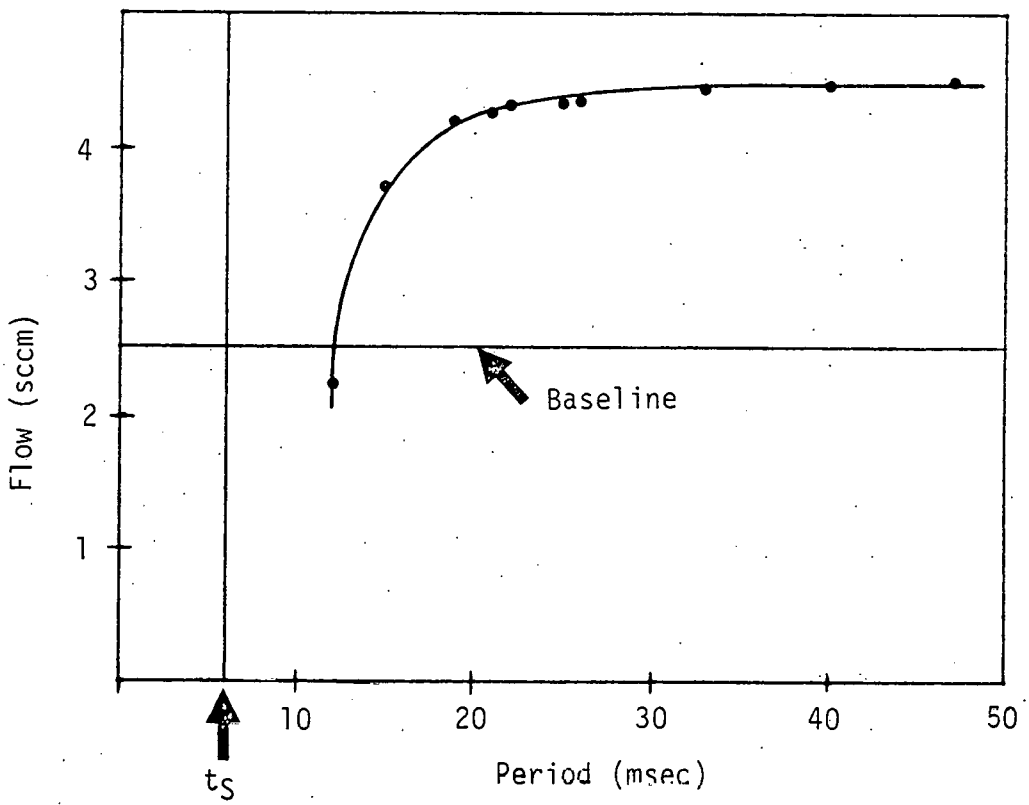


Fig.10. Krypton gas usage as a function of period ($P=t_S + t_T$) with $t_S$ = 6 msec, $E_S$ = $E_T$ = 2500 eV, B = 5 mA/cm$^2$. As NMTAR decreases, the gas usage also decreases until there is not a net deposition. As P is decreased farther, gas is released from the substrate indicating a net removal of previously deposited material. Baseline flow is the system throughput with substrate power supply off. For this data $Bt_S \ll N_{TS}$.

inspection, all of the substrate surface is trapping gas at P=50 msec. At P=16 msec, the center portion of the substrate is still trapping gas, but near the ends, gas is being released as the area of the substrate with a net deposition decreases. At P=14 msec, the net gas usage is less than zero indicating most of the surface has about zero deposition rate, but near the ends there is a net removal. By decreasing P to 6 msec ($t_T$=0), the substrate etch condition would be reached.

Experimental trapping coefficient versus ion energy are plotted in figures 11 and 12 for iron and nickel using square-wave bias. The data is given in Tables IV and V. The solid lines are estimates of what the sticking coefficient vs ion energy curve would be for $t_S$=0 and no end effect with a hypothetical equn. for $\rho$ ($\rho = \frac{2}{\lambda} \sin^2(\frac{\pi x}{\lambda})$).

For titaniun and aluminum, the bias voltage was obtained by modifying the output section of a 3-phase, full wave bridge, DC high voltage power supply to obtain the wave forms depicted in figures 2b,c,d. Utilizing the waveform in fig 2b, a sticking coefficient ($\omega_S$) of .1 atoms/ion at a peak bias of 1650eV was obtained for aluminum and $\omega_S$=.08 at a peak bias of 2150eV was obtained for titanium. Utilizing the waveform in fig 2c, $\omega_S$=.12 at 1525eV peak bias was obtained for aluminum. The waveform in fig 2d did not produce adequate trapping because the voltage could not be raised high enough without excessive sputtering of the deposit.

## 5. CONCLUSION

The high rate supported discharge sputtering process is being applied to the problem of storage of $^{85}Kr$ as an alternative to high pressure gas cylinders. Gas concentrations as high as 5.1 at.% in steel with release temperatures in excess of 570°C have been achieved by simultaneously depositing metal atoms and trapping gas ions. For comparison, steel cylinders can accommodate about 40ℓ STP fission krypton/ℓ volume whereas nickel loaded with 5 at.% krypton is about 160ℓ STP/ℓ volume of deposit. There are deficiencies in the process as described which require further examination and improvements. Most notably, to increase the gas content in the majority of the deposit, the substrate should be segmented so that the substrate bias and substrate "on" time can be adjusted appropriately to accommodate the lower deposition rate near the ends of the substrate while maintaining a high trapping rate on the center portion of the substrate. Scale-up is presently limited by the high substrate bias required to obtain $\omega_S$ values > .1 atoms/ion. The limitation is the current rating of the vacuum tube in the switching network. By finding target materials which have high $\omega_S$ values at voltages an order of magnitude lower than those presently used it would be possible to eliminate pulsed biasing since a commensurately lower amount of material would be resputtered from the substrate. Glassey metals fit this requirement and are presently being investigated. Then, instead of trapping gas in a receding surface upon which fresh layers of metal are being deposited, one would be trapping gas in a continuously advancing surface.

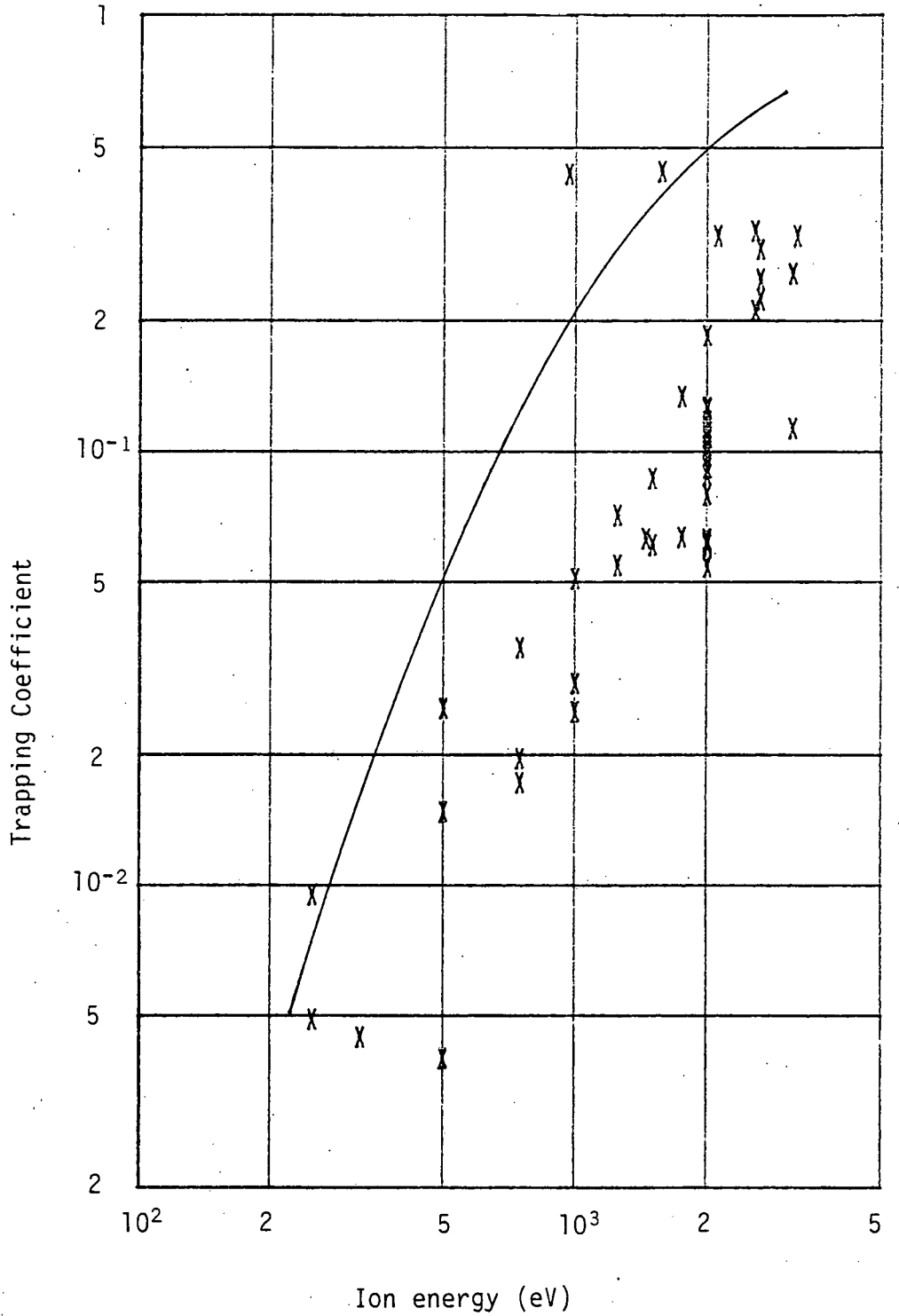


Fig.11. Experimental trapping probability ($\omega_S$) as a function of ion energy for $Kr^+$ ions incident on sputter deposited steel. The solid line is an estimate of $\omega_S$ at $t_S = 0$ and $P >> t_S$ if $\rho = 2\sin^2(\pi x/\lambda)/\lambda$.

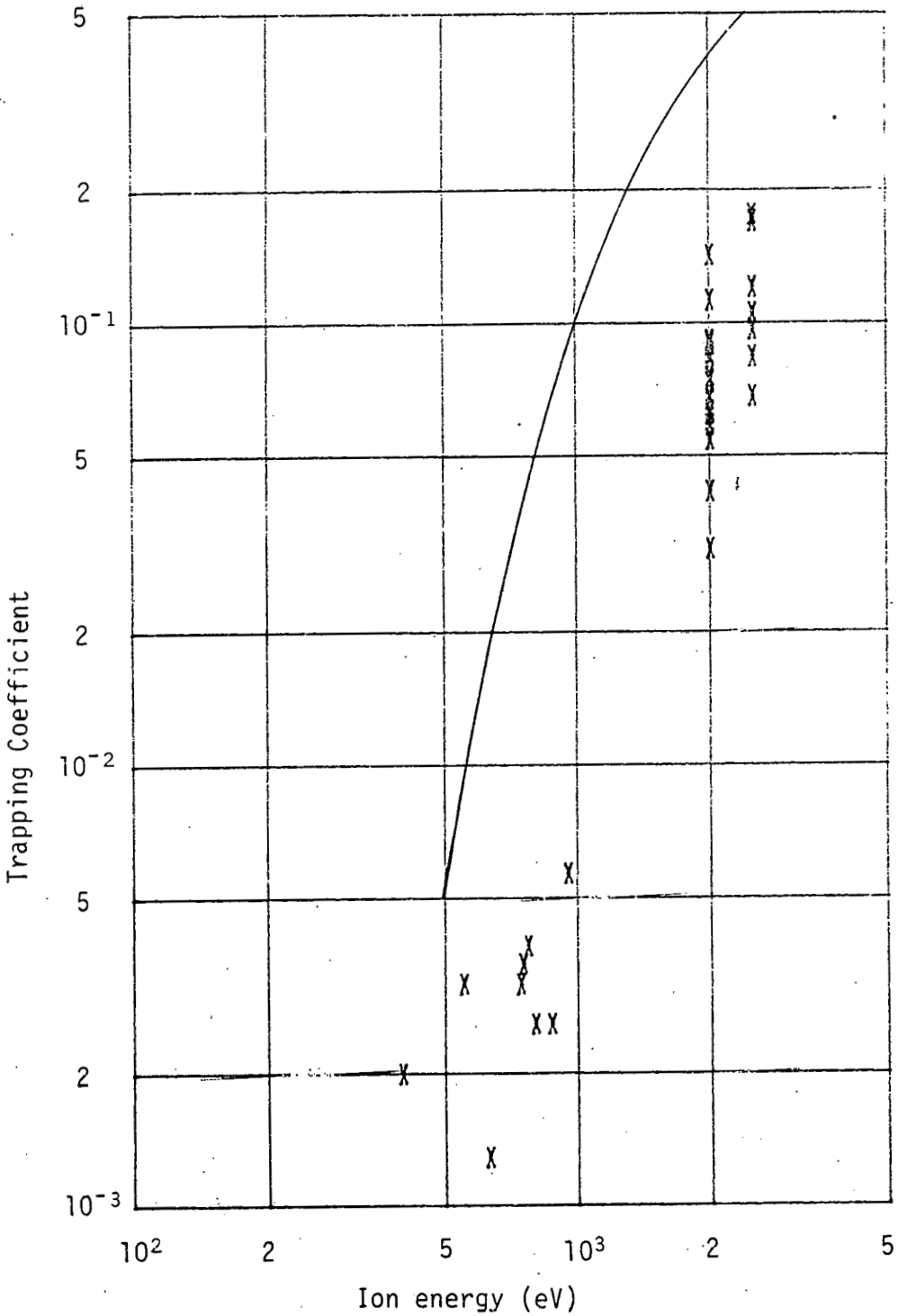


Fig.12. Experimental trapping probability ($\omega_s$) as a function of ion energy for $Kr^+$ ions incident on sputter deposited nickel. The solid line is best estimate of $\omega_s$ at $t_s = 0$ and $P >> t_s$.

TABLE IV. Pulsed Bias Data, Steel

| $E_S$ (ev) | $t_S$ (sec) | $E_T$ (ev) | $t_T$ (sec) | R atoms/cm$^2$/sec | B ions/cm$^2$/sec | P |
|---|---|---|---|---|---|---|
| 3143 | 0.0055 | 2500 | 0.0175 | 1.28E+16 | 3.74E+17 | 0.0175 |
| 3143 | 0.0007 | 2500 | 0.0049 | 1.35E+16 | 4.17E+17 | 0.0049 |
| 323 | 0.0009 | 2500 | 0.0025 | 1.00E+16 | 1.25E+16 | 0.0025 |
| 964 | 0.0002 | 2500 | 0.0025 | 8.94E+15 | 2 55E+17 | 0.0025 |
| 1571 | 0.0003 | 2500 | 0.0025 | 9.45E+15 | 3.42E+17 | 0.0025 |
| 2004 | 0.0004 | 2500 | 0.0025 | 9.45E+15 | 3.98E+17 | 0.0025 |
| 2643 | 0.0006 | 2500 | 0.0025 | 9.91E+15 | 4.30E+17 | 0.0025 |
| 3214 | 0.0003 | 2500 | 0.0025 | 1.41E+16 | 4.36E+17 | 0.0025 |
| 2643 | 0.0004 | 2500 | 0.0025 | 8.44E+15 | 3.24E+17 | 0.0025 |
| 2571 | 0.0003 | 2500 | 0.0025 | 1.43E+16 | 4.55E+17 | 0.0025 |
| 2571 | 0.0005 | 2500 | 0.0025 | 1.93E+16 | 6.72E+17 | 0.0025 |
| 2643 | 0.0005 | 2500 | 0.0025 | 2.18E+16 | 8.90E+17 | 0.0025 |
| 160 | 0.1000 | 2000 | 0.1000 | <5.04E+16 | 1.25E+16 | 0.1000 |
| 168 | 0.1000 | 2000 | 0.1000 | <7.13E+16 | 1.25E+16 | 0.1000 |
| 500 | 0.3200 | 500 | 2.0000 | 3.53E+16 | 1.25E+16 | 2.3200 |
| 750 | 0.3200 | 750 | 2.0000 | 3.49E+16 | 5.38E+16 | 2.3200 |
| 1000 | 0.3200 | 1000 | 2.0000 | 3.39E+16 | 7.61E+16 | 2.3200 |
| 1450 | 0.3200 | 1500 | 2.0000 | 2.07E+16 | 1.16E+17 | 2.3200 |
| 250 | 0.3200 | 250 | 2.0000 | 2.87E+16 | 1.25E+16 | 2.3200 |
| 500 | 0.3200 | 500 | 2.0000 | 2.81E+16 | 3.72E+16 | 2.3200 |
| 750 | 0.3200 | 750 | 2.0000 | 2.81E+16 | 4.93E+16 | 2.3200 |
| 1000 | 0.3200 | 1000 | 2.0000 | 2.57E+16 | 6.72E+16 | 2.3200 |
| 1250 | 0.3200 | 1250 | 2.0000 | 1.65E+16 | 8.06E+16 | 2.3200 |
| 1500 | 0.3200 | 1500 | 2.0000 | 2.13E+16 | 1.16E+17 | 2.3200 |
| 1750 | 0.3200 | 1750 | 2.0000 | 2.76E+16 | 1.57E+17 | 2.3200 |
| 2000 | 0.3200 | 2000 | 2.0000 | 3.09E+16 | 2.19E+17 | 2.3200 |
| 250 | 0.5100 | 2500 | 3.1300 | 1.46E+16 | 1.25E+16 | 3.6400 |
| 500 | 0.5100 | 2500 | 3.1300 | 1.60E+16 | 3.72E+16 | 3.6400 |
| 750 | 0.5100 | 2500 | 3.1300 | 1.82E+16 | 5.82E+16 | 3.6400 |
| 1000 | 0.5100 | 2500 | 3.1300 | 1.84E+16 | 8.51E+16 | 3.6400 |
| 1250 | 0.5100 | 2500 | 3.1300 | 1.94E+16 | 1.25E+17 | 3.6400 |
| 1500 | 0.5100 | 2450 | 3.1300 | 2.05E+16 | 1.61E+17 | 3.6400 |
| 1750 | 0.5100 | 2450 | 3.1300 | 1.95E+16 | 2.37E+17 | 3.6400 |
| 2000 | 0.5100 | 2450 | 3.1300 | 1.95E+16 | 2.24E+17 | 3.6400 |
| 2000 | 0.5100 | 2450 | 3.1300 | 2.87E+16 | 1.61E+17 | 3.6400 |
| 2000 | 0.5100 | 2450 | 3.1300 | 2.98E+16 | 1.70E+17 | 3.6400 |
| 2000 | 0.4100 | 2450 | 3.2300 | 2.98E+16 | 2.24E+17 | 3.6400 |
| 2000 | 0.3100 | 2450 | 3.3300 | 2.98E+16 | 2.06E+17 | 3.6400 |
| 2000 | 0.2100 | 2450 | 3.4300 | 2.98E+16 | 2.06E+17 | 3.6400 |
| 2000 | 0.6100 | 2450 | 3.0300 | 2.98E+16 | 1.97E+17 | 3.6400 |
| 2000 | 0.4100 | 2450 | 3.2300 | 2.98E+16 | 2.24E+17 | 3.6400 |
| 2000 | 0.4600 | 2450 | 3.1800 | 2.98E+16 | 2.24E+17 | 3.6400 |
| 2000 | 0.3600 | 2450 | 3.2800 | 2.98E+16 | 2.24E+17 | 3.6400 |
| 2000 | 0.3600 | 2450 | 3.1800 | 2.98E+16 | 2.24E+17 | 3.5400 |
| 2000 | 0.3600 | 2450 | 3.0800 | 2.98E+16 | 2.24E+17 | 3.4400 |
| 2000 | 0.3600 | 2450 | 2.9800 | 2.98E+16 | 2.24E+17 | 3.3400 |
| 2000 | 0.3600 | 2450 | 2.6800 | 2.98E+16 | 2.24E+17 | 3.0400 |
| 2000 | 0.3600 | 2450 | 2.3800 | 2.98E+16 | 2.24E+17 | 2.7400 |
| 2000 | 0.3600 | 2450 | 1.9800 | 2.98E+16 | 1.61E+17 | 2.3400 |

TABLE V. Pulsed Bias Data, Nickel

| $E_S$ | $t_S$ | $E_T$ | $t_T$ | R | B | P |
|---|---|---|---|---|---|---|
| 2000 | 1.3200 | 2400 | 2.6800 | 3.28E+16 | 2.74E+17 | 4.0000 |
| 2000 | 1.2000 | 2400 | 2.8000 | 3.28E+16 | 3.36E+17 | 4.0000 |
| 2000 | 1.0000 | 2400 | 3.0000 | 3.28E+16 | 3.67E+17 | 4.0000 |
| 2000 | 0.8000 | 2400 | 3.2000 | 3.32E+16 | 3.67E+17 | 4.0000 |
| 2000 | 0.6000 | 2400 | 3.4000 | 3.28E+16 | 3.67E+17 | 4.0000 |
| 2000 | 0.6000 | 2400 | 2.4000 | 3.20E+16 | 4.79E+17 | 3.0000 |
| 2000 | 0.6000 | 2400 | 1.9000 | 3.28E+16 | 4.92E+17 | 2.5000 |
| 2000 | 0.4000 | 2400 | 2.1000 | 3.28E+16 | 4.86E+17 | 2.5000 |
| 2000 | 0.3000 | 2400 | 2.2000 | 3.28E+16 | 4.61E+17 | 2.5000 |
| 2000 | 0.5000 | 2400 | 2.0000 | 3.28E+16 | 4.92E+17 | 2.5000 |
| 2000 | 0.5000 | 2400 | 1.8000 | 3.28E+16 | 5.23E+17 | 2.3000 |
| 2000 | 0.5000 | 2400 | 1.7000 | 3.28E+16 | 5.54E+17 | 2.2000 |
| 2000 | 0.5000 | 2400 | 1.6000 | 3.28E+16 | 5.35E+17 | 2.1000 |
| 2000 | 0.5000 | 2400 | 1.6500 | 3.32E+16 | 5.42E+17 | 2.1500 |
| 2000 | 0.5000 | 2400 | 1.6500 | 4.28E+16 | 5.98E+17 | 2.1500 |
| 2000 | 0.4000 | 2400 | 0.8600 | 4.24E+16 | 8.22E+17 | 1.2600 |
| 2000 | 0.4000 | 2400 | 0.9600 | 5.66E+16 | 8.03E+17 | 1.2600 |
| 2000 | 0.3000 | 2400 | 0.6500 | 5.66E+16 | 9.15E+17 | 0.9500 |
| 2000 | 0.2900 | 2400 | 0.6600 | 5.66E+16 | 8.97E+17 | 0.9500 |
| 2000 | 0.3000 | 2400 | 0.6500 | 6.08E+16 | 9.28E+17 | 0.9500 |
| 770 | 0.3700 | 2500 | 0.4200 | 6.26E+16 | 9.34E+16 | 0.7900 |
| 950 | 0.3700 | 2500 | 0.4200 | 6.26E+16 | 1.37E+17 | 0.7900 |
| 400 | 0.8000 | 2500 | 0.5200 | 6.26E+16 | 6.23E+16 | 1.3200 |
| 750 | 0.2700 | 2500 | 0.5200 | 6.26E+16 | 6.23E+16 | 0.7900 |
| 550 | 0.2700 | 2500 | 0.5200 | 6.26E+16 | 5.60E+16 | 0.7900 |
| 740 | 0.2700 | 2500 | 0.5200 | 6.26E+16 | 5.60E+16 | 0.7900 |
| 630 | 0.3700 | 2500 | 0.4200 | 6.26E+16 | 3.11E+16 | 0.7900 |
| 870 | 0.3700 | 2500 | 0.4200 | 6.26E+16 | 6.23E+16 | 0.7900 |
| 800 | 0.3700 | 2500 | 0.4200 | 6.26E+16 | 6.23E+16 | 0.7900 |
| 2500 | 0.4600 | 2400 | 0.6300 | 4.73E+16 | 1.12E+18 | 1.0900 |
| 2500 | 0.0000 | 2500 | 0.0270 | 3.43E+16 | 9.03E+17 | 0.0330 |
| 2500 | 0.0060 | 2500 | 0.0160 | 3.43E+16 | 8.09E+17 | 0.0220 |
| 2500 | 0.0060 | 2500 | 0.0130 | 3.43E+16 | 7.47E+17 | 0.0190 |
| 2500 | 0.0060 | 2500 | 0.0160 | 3.43E+16 | 8.09E+17 | 0.0220 |
| 2500 | 0.0060 | 2500 | 0.0150 | 3.43E+16 | 7.78E+17 | 0.0210 |
| 2500 | 0.0060 | 2500 | 0.0190 | 3.43E+16 | 8.16E+17 | 0.0250 |
| 2500 | 0.0060 | 2500 | 0.0270 | 3.43E+16 | 8.72E+17 | 0.0330 |
| 2500 | 0.0060 | 2500 | 0.0340 | 3.43E+16 | 8.84E+17 | 0.0400 |
| 2500 | 0.0060 | 2500 | 0.0410 | 3.43E+16 | 8.97E+17 | 0.0470 |
| 2500 | 0.0060 | 2500 | 0.0090 | 3.43E+16 | 5.29E+17 | 0.0150 |
| 2500 | 0.0060 | 2500 | 0.0060 | 3.43E+16 | -1.25E+17 | 0.0120 |
| 2500 | 0.0060 | 2500 | 0.0200 | 3.43E+16 | 8.28E+17 | 0.0260 |

ACKNOWLEDGMENTS

We greatfully acknowledge the contributions of R. A. Lundgren in apparatus design, E. N. Greenwell in pulsing circuitry development and the technical support of J. W. Johnston, E. L. McDonald, W. W. Roberts and R. F. Stratton.

REFERENCES

1. J. R. Coleman and R. Liberace, "Nuclear Power Production and Estimated $^{85}Kr$ Levels", Radiological Health Data and Reports, Vol. 7, pp. 615-621, 1966.

2. "Environmental Radiation Protection Standards for Nuclear Power Operations", Federal Register, Vol. 42, No. 9, Title 40, part 190, January 13, 1977.

3. M. Laser, "Separation, Storage and Disposal of Krypton-85 Status and Projects", Paper prepared for the IAEA Technical Committee on Removal, Storage and Disposal of Gaseous Radionuclides from Airborne Effluents, Sept. 1976, GERHTR-177.

4. K. B. Blodgett, T. A. Vanderslice, J. Appl. Phys. 31 (1960)1017.

5. R. S. Nelson, M. J. Smith: Storage of $^{85}Kr$ in a Metal Matrix; Harwell-prospectus.

6. R. A. Brown, M. Hoza, and D. A. Knecht, "$^{85}Kr$ Storage by Zeolite Encapsulation", Proc. Fourteenth ERDA Air Clean. Conf., 1976, CONF-760822, NTIS, Springfield, VA, Vol. 1, pp. 118-131, February 1977.

7. E. D. McClanahan, R. W. Moss, N. Laegreid, J. W. Patten, R. Busch, M. A. Bayne, E. N. Greenwell, "State-of-the-Art for High-Rate Sputter Deposition", Presented at the Government-Industry Workshop on Alternatives for Cadmium Electroplating in Metal Finishing, National Bureau of Standards, Gaithersburg, MD, Oct 4-6, 1977.

8. G. Carter, J. S. Colligon, J. H. Leck, "Ion Sorption in the Presence of Sputtering", Proc. Phys. Soc., Vol. 79(1962)299.

9. D. Rosenberg, G. K. Wehner, J. Appl. Phys., V. 33(5), 1962, p.1842.

10. J. A. Davies, B. Domeij, J. Uhler, Arkiv. f. Fysik. 24(1963), 377.

11. O. Almen, G. Bruce, J. Nucl. Instrum. Methods 11(1961), 257.